Polymer Bulletin 62, 99–110 (2009)
DOI 10.1007/s00289-008-1014-7

Polymer Bulletin

Morphology and Osteogenetic Characteristics of Polyamide/NanoHydroxyapatite Biocomposites

L. I. Castelan-Velazco, J. Mendez-Nonell, S. Sanchez-Valdes, and L. F. Ramos-deValle (✉)

Centro de Investigación en Química Aplicada (CIQA), P.O. Box 379, Saltillo, Coahuila, 25253, México

E-mail: devalle@ciqa.mx; Fax: 52 (844) 4389839

Received: 20 August 2008 / Revised version: 1 October 2008 / Accepted: 4 October 2008
Published online: 20 October 2008 –

Summary

The effect of shear or time of shearing – as exerted by different screw configurations – upon the nano hydroxyapatite (n-HA) dispersion, during the twin screw extrusion processing for the preparation of PA6-66/n-HA composites, was investigated. Three different screw configurations, designated as medium, high and very high shear, were used. A noticeable improvement in the n-HA dispersion, attributed to the increasing shear exerted upon the melt during mixing in the TSE, was observed. Crystallization and thermal behavior of n-HA reinforced PA6-66 composites were studied by X-ray diffraction (XRD), differential scanning calorimetry (DSC) and thermogravimetric analysis (TGA). An increase in the crystallization temperature, accompanied by a decrease in percent crystallinity with the addition of n-HA to the PA6-66 matrix was observed. That is, n-HA acted as a nucleating agent and enhanced the crystallization rate. In addition, it was observed that the n-HA promoted the occurrence of the Brill transition. The decomposition temperature increased with the addition of n-HA. The PA6-66/ n-HA nanocomposite was thereafter, immersed in simulated body fluid (SBF) and the generation of a new calcium phosphate layer on the nanocomposite surface was monitored by SEM, FTIR and Atomic Absorption. The Ca/P ratio in the forming apatite layer started at a low value, ca. 1.3, which corresponds to octacalcic phosphate, but increased with the immersion time to 1.6, which corresponds to carbonated apatite.

Introduction

Human bone tissue is a kind of composite mainly composed of nano-apatite crystals (around 65 wt%) and collagen matrix [1]. Hydroxyapatite has been used for orthopaedic/ dental implants and for filling of bone defects because of its similar chemical composition and structure to the mineral phase of human bone; and due to its biocompatibility and bioactivity, it can bond with living tissue through osteo-conduction mechanisms [2]. However, due to low fracture toughness, HA cannot serve as a bulk implant material under high physiological loading conditions. The high elastic modulus of bioceramics and biometals may result in stress-shielding [3], which

should be avoided, since living bone must be under some mechanical load to prevent atrophy and remain healthy. Therefore, the implantable material properties should match the mechanical characteristics of the surrounding bone tissue. Therefore, development of biocomposites with good mechanical properties, excellent bioactivity and biocompatibility similar to natural bone to meet the need of hard tissue repair has been a hot topic for many years. An ideal material for bone repair must be biocompatible and bioactive, able to initiate osteogenesis, and should have mechanical properties and composition similar to the bone. In order to obtain an advanced mechanical performance of the bioactive composite, bioceramic particles were usually incorporated into the polymer matrix using conventional plastics processing technology [4]. Various composite systems have been explored as bone substitute materials, including HA reinforced polyethylene, polylactide, collagen and others [5]. Most studies report using less than 45% of HA due to the large size of the HA particles used and the melting process. This can restrict the bioactivity of the composite [6]. In some other reported studies the organic matrix used is not a polar polymer or their molecular structure is not similar to collagen in natural bone. This can restrict the interface binding and the mechanical behavior of the composites [7]. The first n-HA/PA66 biocomposites for bone repair was reported by Yubao Li [8] in which they found mechanical properties close to natural bone. Recent studies on animals and clinical experiments have proved that the n-HA/PA66 composites have good compatibility to bone and can bond directly to bone. It is well known that nano particles are more difficult to disperse than micro particles, mainly because of their higher surface area and very small particle size that promote the particle aggregation. It can be affirmed that a nanocomposite with poor nanoparticle dispersion is going to have low mechanical properties due to the formation of stress concentration regions or weak points on the polymer matrix by the nano particle aggregates that initiates and propagates cracks. The chemical and physical properties of polymer materials and polymeric matrix composites are strongly influenced by their thermal and crystallization behavior. Thermal studies of polyamide layered silicate nanocomposites (PLSN) have been carried out extensively [9]. Until now, only few studies have been reported on the thermal and crystallization behaviour of n-HA/PA66 biocomposites [10]. In this study, nano-hydroxyapatite (n-HA), which is similar to bone apatite and a polar polymer, such as polyamide (PA6-66), which have carboxyl and amide groups, like collagen, are used to make a biomimetic composite.
The effect of shear, --as exerted by different screw configurations-- on the dispersion and morphology of nano-hydroxyapatite/PA6-66 biocomposites is examined. The crystallization and thermal behavior of n-HA reinforced polyamide biocomposites, has also been studied. Finally the formation of a new hydroxyapatite layer on the nanocomposite surface was investigated. The main advantage of using the PA6-66 copolymer over the PA6 or PA66 should be its much lower processing temperature.

Experimental

Materials

Nano-hydroxyapatite (n-HA), obtained directly from animal bone calcination, with a stequiometric Ca/P value of 1.67 and an average particle size of 84 nm was used. A copolymer of Polyamides 6 and 66, ULTRAMID C33 from BASF was used. This polymer consists of 80% PA6 and 20% PA66 with a melting temperature of 195°C.

Preparation of n-HA/PA6-66 nanocomposites

The n-HA/PA6-66 nanocomposites were prepared via melt mixing and pelletized using a Werner and Pfleiderer co-rotating twin screw extruder (TSE) model ZSK-30, with 10 wt% of n-HA at a 240°C and 200 rpm. Three mixing screw configurations were used. The level of shear in each screw configuration was changed by modifying the number of kneading elements, which directly affect the time of shearing exerted upon the sample, as well as the number of reverse conveying elements, which directly affect the residence time, and as a consequence, the time during which, shear is exerted upon the sample. The screw configurations are denoted as medium (1), high (2), and very high (3) residence time (RT) configurations. The three screw configurations are described in **Table 1**. Sections 1, 2, 5, 7 and 9, are identical in all 3 screw configurations used. In High -vs- Medium Residence Time Configurations: The High RT has two kneading sections (sections 3 and 6), longer (42 mm) than those in the Medium RT (28 mm). In Very High -vs- High RT Configurations: The Very High RT has a Reverse Conveying Section (section 4), longer (20 mm) than those in the Medium and High RT (10 mm); and has an additional Reverse Conveying Section (section 8; 10 mm long), where the others have a normal conveying section. The conveying elements are designated as: 20/10, which indicates an element with pitch and axial length equal to 20 and 10 mm, respectively. LH means a reverse element. The kneading elements are designated as: 45/5/28, which indicates an element with 5 ellipsoids, with tips shifted 45 degrees with respect to the previous one, and 28 mm of axial length (that is; each ellipsoid would be 28/5 = 5.6 mm thick). **Figure 1** shows the description of these three screw configurations.

Table 1. Incorporation methods and steps of mixing

Convey Section	Kneading Section	Kneading Section	Reverse Convey Section	Convey Section	Kneading Section	Forward Kneading Section	Forward-Reverse Convey Section	Convey Section
Screw Sections:								
1	2	3	4	5	6	7	8	9
Medium Residence Time								
Convey	knead	45/5/28	20/10LH	Convey	45/5/28	knead	Convey	Convey
High Residence Time								
Convey	knead	**45/5/42**	20/10LH	Convey	**45/5/42**	knead	Convey	Convey
Very High Residence Time								
Convey	knead	**45/5/42**	20/20LH	Convey	**45/5/42**	knead	20/10LH	Convey

After being dried at 80°C for 8 h, pellets of the nanocomposites were compression molded into standard test pieces for mechanical tests by using a Hydraulic Press at 220°C and 10 Tons of pressure.

Characterization of n-HA/PA6-66 nanocomposites

X-ray diffraction of the nanocomposites was performed in a Siemens D5000 using CuKa X-ray radiation. The X-ray samples were obtained from compression moldings. The XRD patterns were scanned in the 2 θ range from 5 to 40 degrees at a rate of

0.6 θ/min. The melting and crystallization behavior of the samples was studied using a TA instruments model 2920 differential scanning calorimeter (DSC). The thermograms were obtained at a temperature range from 5 to 180°C with a heating and cooling rate of 10°C/min in a nitrogen atmosphere. The samples of PA polymer with and without n-HA were dried at 80°C for 72 h to eliminate the humidity from the samples.

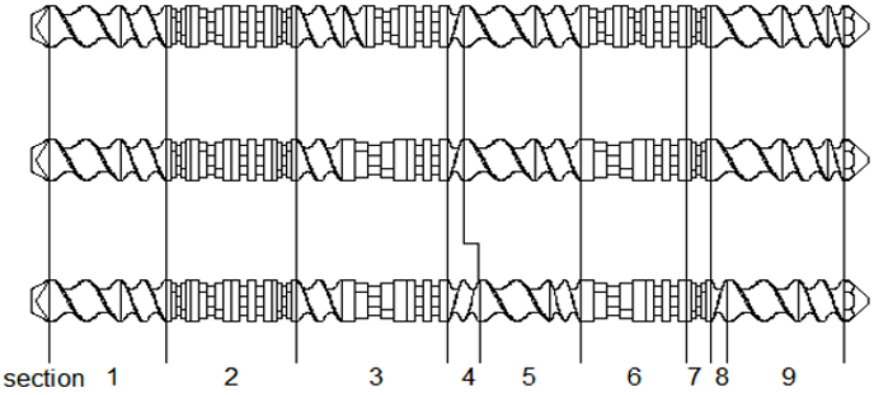

Figure 1. Diagrams of the screw configurations used in this study, depicting the 9 different sections described in Table 1.

In order to determine the thermal stability and decomposition temperature of the raw materials and the nanocomposites, thermogravimetric analysis (TGA) was used. TGA was carried out with a Dupont Instruments TGA-951 analyzer. The samples were analyzed at a heating rate of 10°C/min under a nitrogen flow. The samples of polyamide polymer with and without n-HA were dried at 80°C for 72 h in order to eliminate the humidity from the samples. Tensile properties of the polyamide and the nanocomposites were measured in a United Tensile Tester 3M-10 machine, fitted with a 450 kg load cell at an extension rate of 5 mm/min. All tests were performed in accordance to ASTM D638. Six test specimens were tested for each data point and the average was taken as the result. The in-vitro bioactivity of the nanocomposites was studied using a simulated body fluid (SBF), which was prepared by dissolving the reagents listed on **Table 2** in deionised water at 37°C, maintaining a pH of 7.25. The simulated body fluid was prepared by dissolving various reagents, such as; NaCl, $NaHCO_3$, KCl, K_2HPO_4-$3H_2O$, $MgCl_2$-$6H_2O$, $CaCl_2$, and Na_2SO_4 into de-ionized water. This SBF solution is buffered at pH 7.25 by tris-(hydroxy-methyl)-aminomethane [$(CH_2OH)_3{\equiv}C\text{-}NH_2$] and 1M hydrochloric acid (HCl), at 36.5°C. The frequently used SBF in literature differs from that of blood plasma by high content of Cl-, and low content of HCO_3- ions [12]. This simulated body fluid is very similar to human blood plasma composition and has been used with excellent results in some reported bioactivity studies [11]. The nanocomposite samples were immersed in 50 ml of SBF in a closed plastic bottle and kept at 37°C for 1, 3, 5, 7, 14 and 21 days. After each time, the nanocomposites were washed in deionised water, dried at 30°C for 12 hours and stored in a drier. The Ca/P ratio of the HA layer forming on the surface of the sample was determined by Atomic Absorption Spectroscopy using a Termo Jarell Ash Spectrometer. The SBF was stored at 5°C and was continuously analyzed in order to determine the Ca and P concentration. The characteristic IR bands of the HA

and PA and the nanocomposites during the bioactivity tests were determined through FTIR by using a Thermo-Nicolet Magna 550 IR analyzer. The FTIR of the raw materials was performed on thin films obtained by hot-pressing and for the nanocomposites submitted to bioactivity tests, the samples were first burned at 700°C in order to eliminate the PA polymer and the remaining ceramic ashes were prepared and analyzed in the same way as described for the raw materials. The surface morphology and the elemental surface composition of the nanocomposites were analyzed on fractured samples of tensile specimens by scanning electron microscopy with EDS (SEM-EDS) Model Top Con 510 SM. The samples were fractured in liquid nitrogen after 15 to 20 min of freezing. The fractured surfaces were treated with Au/Pd alloy. The reported SEM micrographs were selected from at least 5 observations.

Table 2. Reagents Used for the SBF Preparation

Reactive	Content/ 1L of H_2O	Reactive	Content/ 1L of H_2O	Reactive	Content/ 1L of H_2O
NaCl	7.995 g	K_2HPO_4 $3H_2O$	0.228 g	Na_2SO_4	0.071 g
$NaHCO_3$	0.353 g	$MgCl_2$ $6H_2O$	0.305 g	$(CH_2OH)_3{\equiv}C\text{-}NH_2$	6.055 g
KCl	0.224 g	$CaCl_2$	0.278 g	HCl	60 ml

Results and discussion

Effect of screw configuration

Figure 2 presents the SEM micrographs of PA6-66/ n-HA nano-composites, with 10wt% of HA, showing the effect of time of shearing upon the hydroxyapatite (n-HA) dispersion during melt mixing in the twin screw extruder. It can be clearly observed that the samples show different dispersion degrees, most certainly due to the different shearing time (*the only variable*) applied by the three different screw configurations. **Figure 2-a** shows a sample prepared with the medium RT configuration, where many particle aggregates can be observed, indicative of poor mixing and poor dispersion. **Figure 2-b** shows a sample prepared with the high RT configuration, where only a few particle aggregates and better particle dispersion can be observed, this is mostly due to the higher shearing time applied with this configuration. Finally, **Figure 2-c** shows a sample prepared with the very high RT configuration, where there appears to be no particle aggregates, on the contrary, a morphology of fine n-HA seeds throughout the nanocomposite is observed. As mentioned, this is mostly due to the higher shearing time applied with this configuration. This noticeable improvement in comminution and dispersion is attributed to the increasing shear exerted upon the sample during melt mixing in the TSE. Attaining the best possible dispersion of the n-HA into the polymer matrix is very important in order to achieve a highly homogeneous product with the best mechanical and bioactive properties [13,14]. Therefore, direct mixing of n-HA with PA6-66 in a TSE is an effective method to prepare a homogeneous nano-composite with high n-HA content. In TSE, most of the mixing occurs during passing through the kneading blocks, as a result of the high shearing time applied in these sections. The main goal in the dispersion process is to reduce the size of the particle aggregates and uniformly distribute the smaller particles into the polymer matrix. The description of the three screw configurations used in this

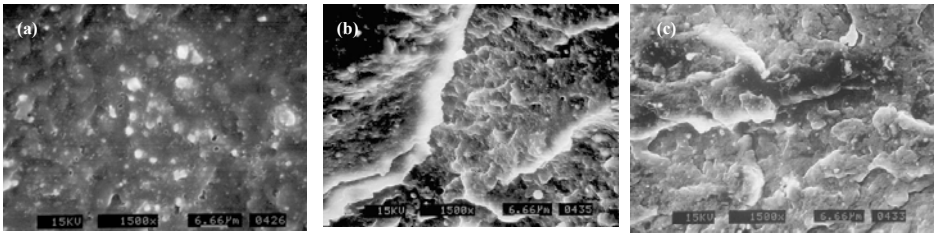

Figure 2. SEM micrographs for the n-HA/PA6-66 nanocomposites (10wt% n-HA), prepared with the: (a) medium, (b) high and (c) very high residence time screw configurations.

study is presented in **Table 1** and **Figure 1**. The very high residence time configuration produced the best n-HA particle dispersion.

Effect of n-HA on crystallization behavior

Figure 3 shows the x-ray diffraction patterns of the PA6-66 copolymer and the PA6-66/ n-HA nanocomposite with 10wt% n-HA. The diffraction pattern of PA6-66 shows only one diffraction peak attributed to the gamma γ crystalline phase, whereas the diffraction pattern for the nHA/PA6-66 nanocomposite shows two diffraction peaks that indicate the presence of (gamma) γ and (alpha) α crystalline phases. In addition, from the magnitude of the area under the curve, it can be inferred that the pure polyamide has a relatively higher crystalline content. It is observed that the intensity of the main peak of PA6-66 at 2 θ around 20-24 θ decreases. This indicates a decrease in crystalline content, which can be explained considering that the new hydrogen bonds, between the polyamide and the hydroxyapatite would affect the plane structure of PA6-66, restricting the polyamide crystallite formation, resulting therefore in a decrease of the PA6-66 crystallinity [15]. The crystalline content of the pure PA6-66 and the n-HA/PA6-66 nanocomposite was determined, from the XRD patterns, as 49% and 42% respectively, measuring the area under the curves considering the thickness of the samples and subtracting the amorphous halos.
Figure 4 presents the DSC curves for the crystallization of the PA6-66 and the n-HA/PA6-66 nanocomposite with 10wt% of n-HA, at a cooling rate of 10°C/min. The nanocomposite was prepared using the very high RT configuration. It can be observed that during cooling, the crystallization of PA6-66 in the nanocomposite

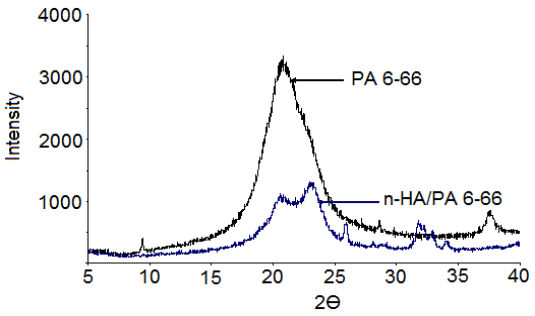

Figure 3. X-ray diffraction patterns of the PA6-66 and n-HA/PA6-66 nanocomposite with 10 wt% of n-HA.

occurs at higher temperature than in the pure polymer. The temperature at the peak maximum was 166°C for the PA6-66 in the nanocomposite, whereas it was 159°C for the pure PA6-66. This increase in the crystallization temperature of the polyamide composite compared to that of the neat polyamide clearly indicates the nucleating agent role of the n-HA; which apart from inducing crystallization at a higher temperature, promotes a more rapid crystallization rate. In addition, it appears that n-HA specifically promotes the formation of the (alfa) α crystalline phase. This coincides with reports that the half-life time of crystallization ($t_{1/2}$) of polyamide is higher than that of their n-HA composites [10]. However, it was found that the addition of n-HA decreases the crystalline content of PA6-66. This latter effect can be attributed to the external confinement introduced by the solid walls of the n-HA, restricting the lamellar growth in the nanocomposite.

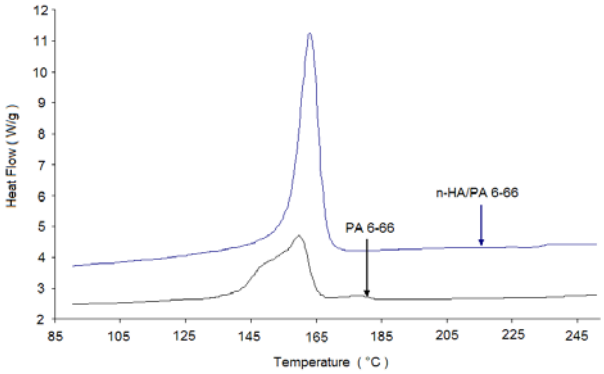

Figure 4. DSC curves of PA6-66 and 10wt% n-HA/PA6-66 nanocomposite, at a cooling rate of 10°C/min

Figure 5 shows the DSC melting curves of PA6-66 and the n-HA/PA6-66 nanocomposite. It is observed that the pure PA6-66 curve shows one melting peak, at 198°C, whereas the n-HA/PA6-66 nanocomposite shows two melting peaks, at 192°C and 197°C. One (197) is related to the melting peak of pure nylon 6-66, whereas the other (192), is due to the change brought about by the nucleating effect of nano-HA upon the crystallization and melting of nylon 6-66. These two melting peaks are a clear indication of the occurrence of the Brill transition, undoubtedly promoted by the presence of the n-HA. Many semicrystalline polymers undergo phase transitions prior to melting [16]. In the case of polyamides, these are known as Brill transition [17]. This Brill transition is easily seen in PA 66, as the two strongest peaks in the wide-angle X-ray diffraction scans merge into a single peak at the Brill transition [17]. NMR confirms these structural changes in both PA 66 and PA 6 [18]. Changes in the physical properties of the semicrystalline polymers during the transitions can be of practical importance [19]. The triclinic crystalline structure of PA66, at room temperature, transforms into a different, also triclinic structure, at a higher temperature, namely, the Brill transition [18]; this high temperature crystalline form is characterized as a pseudo-hexagonal form. A similar monoclinic to monoclinic phase transformation occurs in PA 6 [18].

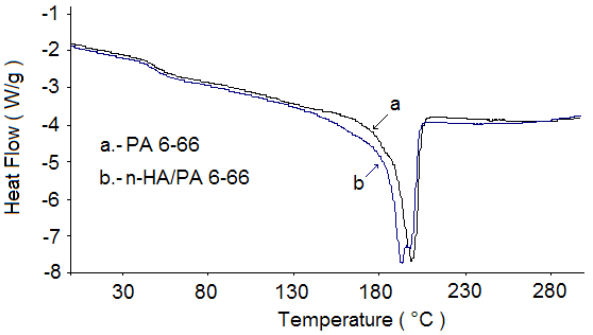

Figure 5. DSC curves of PA6-66 and 10wt% n-HA/PA6-66 nanocomposite at a heating rate of 10°C/min.

Effect of n-HA on thermal behavior

Thermogravimetric curves of PA6-66 and n-HA/PA6-66 nanocomposite with 10wt% n-HA are shown in **Figure 6**. The temperature range used for the analysis was from 10 to 800°C. It can be observed that PA6-66 starts to decompose at a temperature near 370°C. This figure reveals that n-HA/PA6-66 degrades at higher temperature than does the pure PA6-66, i.e. the thermal stability of the composite is higher. The decomposition temperature, at which 50% weight loss occurred, for the PA6-66 is near 455°C whereas that for the n-HA/Pa6-66 composite is 472°C, that is, 17°C higher. The increased stability of the composite compared to PA6-66 may result from the hydrogen bonds between hydroxyl group (-OH) of n-HA and the amide group (-NH-C=O) of PA6-66 matrix, which strengthens the interfacial action [10]. The possible chemical structures of hydroxyapatite-polyamide 6-66 are given in **Diagram 1**. This is in agreement with the results obtained by other authors [8,10].

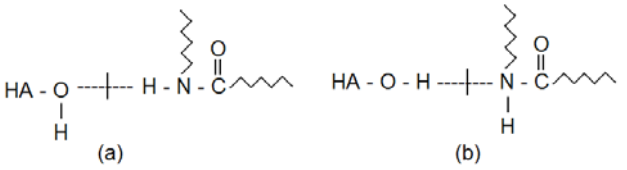

Diagram 1. Presumed hydrogen bonding between the hydroxyl groups of n-HA (-OH) and the amide groups of the PA6-66 matrix (-NH-C=O).

Effect of n-HA on the tensile properties of the nanocomposite

Table 3 shows the effect of n-HA dispersion (melt mixing in the medium and very high RT screw configurations) on the tensile properties of the polyamide composite. It can be observed that the mixing process has an effect. Mixing in the very high RT screw configuration produces “tougher” composites, that is, composites with higher tensile strength at yield and higher modulus, but without negatively affecting its elongation. In addition, the ultimate tensile strength and the tensile modulus of this nanocomposite (112 and 2,620 MPa, respectively), are in the same range of those of natural bone (40-200 MPa and 2-50 GPa, respectively) [20].

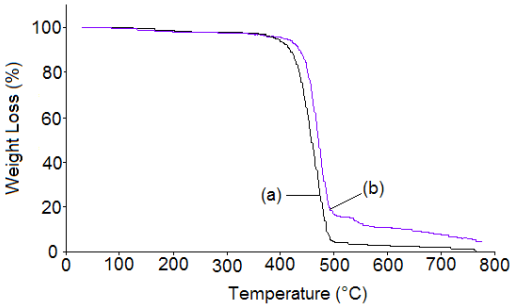

Figure 6. Thermogravimetric curves of (a) PA6-66 and (b) 10%wt n-HA/PA6-66 nano-composite.

Table 3. Tensile Properties of PA6-66 and PA6-66/ n-HA, Showing the Effect of Shearing Time, as Exerted by the Medium and Very High RT Screw Configurations, During Melt Mixing.

	PA6-66	PA6-66/n-HA Screw Config.1*	PA6-66/n-HA Screw Config.3*
Tensile Strength at Break [MPa]	75	96	112
Tensile Modulus [MPa]	2,300	2,550	2,820
Elongation at Yield [%]	6	4	5.5
Elongation at Break [%]	45	30	40

* PA6-66/n-HA nanocomposites, with 10 wt% nano-hydroxyapatite, prepared using the medium (1) and very high (3) RT screw configurations.

Effect of n-HA on the generation of a new HA surface layer

In this case, the studied nanocomposite was the one with 10wt% of n-HA prepared with the very high RT screw configuration. **Figure 7** shows the SEM micrographs of the nanocomposite after being immersed for 1, 3, 4, 7, 14 and 21 days in SBF. It can be observed that the calcium nucleation starts since the very first day. The nuclei formation through the nanocomposite surface can be appreciated. These nuclei formation at the beginning seems to be randomly distributed and as the immersion time is increased, the whole nanocomposite surface is covered with calcium phosphate nuclei (**Fig 7f**). The morphology of the coating layer is of spherical particle aggregates with relatively small crystals, which suggest a high nucleation rate. The formation of new nuclei is apparently preferred to occur on the previously formed apatite particles, forming a cauliflower resembling morphology as can be seen in these micrographs. These results confirm that a calcium phosphate layer, of bone apatite, can efficiently grow on the surface of the composite by incubation of the sample in a solution with an ionic composition similar to human blood plasma. **Figure 8** shows the evolution of the Ca/P ratio of the forming calcium phosphate layer with the immersion time in SBF, as measured by atomic absorption. After one day the Ca/P ratio was 1.3, which is close to the octacalcic phosphate phase. However, as the time in SBF increased, the Ca/P ratio clearly tended to the ratio of the biological or bone apatite of 1.6. This suggests that this octacalcic phosphate phase starts to form at the very beginning and due to the

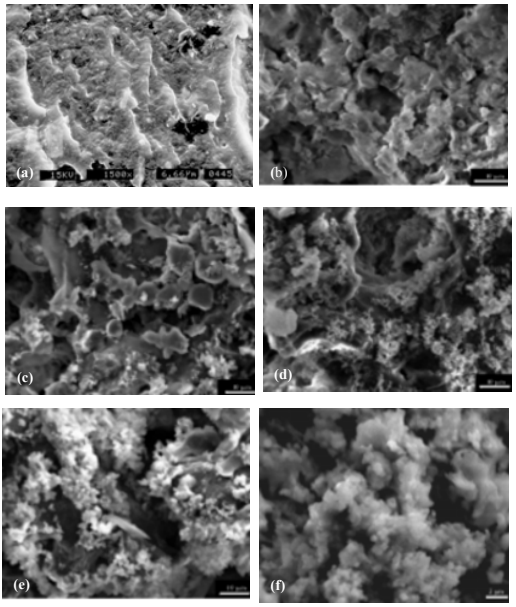

Figure 7. SEM micrographs of the n-HA nanocomposites immersed in a SBF for different periods of time: a) 1 day, b) 3 days, c) 5 days, d) 7 days, e) 14 days and f) 21 days. The magnification for b to f is 2,000X and for a is 1,500X

slight calcium and phosphorous ions saturation, this phase acts as precursor for the formation of carbonated HA.

Figure 9 shows the FTIR spectra of the surface of the PA/HA nanocomposite samples as a function of the time of immersion in the SBF. It can be seen that the absorption peaks at 1060 and 952 cm^{-1}, associated to the PO_4 vibration, noticeably increase with the immersion time. The absorption peak at 1460 cm^{-1} is associated to the C-O stretching which would correspond to the saturation of the carbonate ions in the apatite structure. This suggests that eventually, this coating is mainly formed by carbonated apatite. These results are in agreement with the results obtained by other authors in the coating of different materials with apatite by biomimetic means [21]. It was observed that, during the nanocomposite immersion in the SBF, spherical calcium phosphate nuclei started to form, which started to grow and coat the whole polymer surface. This calcium phosphate layer on the polymer surface was characterized as carbonated apatite. This suggests that, under these conditions, the n-HA/PA6-66 nanocomposite behaves as a bioactive material. Several authors have reported that the process of formation of a Ca-P layer on the surface of a material when immersed in SBF, is an indication of bioactivity and is called a bio-mineralization process [22]. This bio-mineralization process is a simple method in which a non-bioactive surface can be functionalized and transformed into a bioactive surface, or the bioactivity of a bioactive material can be enhanced by this method. As a result of the study and considering the results from other authors [22], it can be assumed that the apatite formation mechanism could be as follows: the HCl in the SBF increases the number of polar groups on the nanocomposite surface which in turn increase their affinity towards the silicate ions, which provide specific sites for the apatite nucleation. As

a result, a very high number of apatite nuclei are formed on the nanomaterial surface during the incubation in SBF. The first forming layer consist of calcium phosphate with a Ca/P ratio lower than 1.5. After which, nucleation and growth of a second layer take place via the consumption of the calcium and phosphate ions from the environment. The initial layer has a Ca/P ratio comparable with the octacalcic phosphate phase, which apparently acts as a precursor of the second layer. As the immersion time is increased, the Ca/P ratio increases until reaching a value of 1.6, which corresponds to a biological apatite.

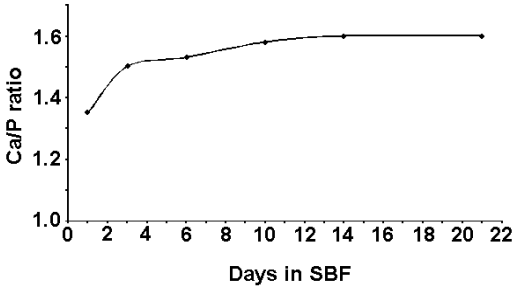

Figure 8. Variation of Ca/P ratio versus time for the nanocomposites immersed in SBF.

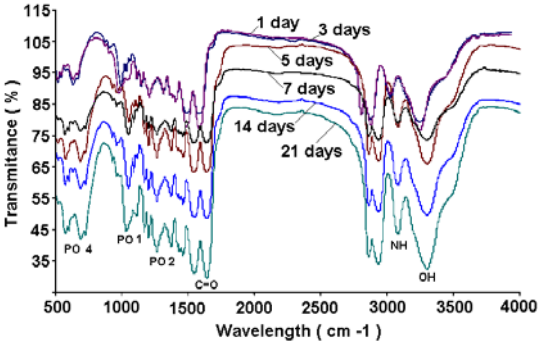

Figure 9. Variation of the FTIR spectra for the nanocomposites immersed in SBF for different periods of time

Conclusions

It was found that the shearing time exerted during melt mixing notably affects the HA dispersion. The screw configuration, designated as the very high residence time, produced the best dispersion; that is, the higher the shear exerted upon the mix, the better the n-HA comminution and dispersion in the polymer. It was also found that the n-HA acts as a nucleating agent, inducing the crystallization of the polyamide at a higher temperature. This increase in Tm was accompanied by a decrease in the percent crystalline content of the polyamide, which was attributed to the restrictions imposed by the confined environment due to the presence of the n-HA. Additionally, the n-HA acted as nucleating agent for the crystallization of the α phase, generating the amply studied Brill transition. TGA showed that the thermal stability of the n-HA/PA6-66 composites is higher than that of PA6-66, which is due to the hydrogen

bonds between the amide group of PA6-66 and hydroxyl group of n-HA. The formation of a biological apatite layer on the surface of PA6-66/n-HA nanocomposites, --prepared via melt mixing-- after immersion in simulated body fluid, was demonstrated. The Ca/P ratio in the apatite layer forming on the nanocomposite surface started at a low value ca. 1.3, which corresponds to octacalcic phosphate, but increased with the immersion time to a value that corresponds to the stequiometric ratio of 1.6, which corresponds to carbonated apatite. During immersion in the SBF, provides the calcium and phosphate ions needed for the new HA formation on the nanocomposite surface.

Acknowledgements. The authors gratefully acknowledge the financial support of CONACyT (SEP-2003-CO2-43983) and the help in the laboratory testing and figure preparation of M. Sanchez-Adame, M. Lozano-Estrada, B. Huerta-Martinez, J. Zamora-Rodriguez, M.C. Gonzalez-Cantu, J. Rodriguez-Velazquez and E. Hurtado-Suarez.

References

1. Watabe N., (1965) Calcif Tissue Int 29:163.
2. Hench LL, Wilson J. (1984) Science 226: 630.
3. Peppas NA, Langer R. (1994) Science 263: 1715.
4. Bonfield W, Grynpas M, Tully A, Bowman J, Abram J. (1981) Biomaterials 2: 185.
5. Du C, Cui F, Feng Q, Zhu X, de Groot K. (1998) J Biomed Mater Res 42: 540.
6. Doyle C, Tanner K E, Anseau N, Bonfield W. (1988) Biomaterials Congress 3: 469.
7. Kelly BS, Dunn RL, Casper RA. Adv. in biomedical polym. New York, (1987) : 77.
8. Xuejiang W, Yubao L, Jie W, Klass de G. (2002) Biomaterials 23: 4787.
9. Qin H, Su Q, Zhang S (2003) Polymer 44: 7533.
10. Zhang X, Li Y, Lv G, Zuo Y, Mu Y. (2006) Polym Degrad Stab 91: 1202.
11. Kokubo T, World Scientific Pub. Co. Singapore (1993): 1.
12. Helebrant A, Jonasova L, Sanda L, (2002) Ceramics-Silikaty 46: 9.
13. Yubao L, Yonggang Y, Jiangqing F, (1999) 4th Asian Symp Biomed Materials, 89.
14. Franzheim O, Stephan M, (1997) SPE ANTEC Tech. Papers, 2591.
15. Vaia RA, Meeting of the American Physical Society, (2000), G22.
16. Turi, Edith A. (1997) Thermal Charac of Poym Mats, Academic Press: New York.
17. Brill, R. J. (1942) Prakt. Chem., 161, 49.
18. Hirschinger, J.; Miura, H.; Gardner, K.; English, A. (1990) Macromolecules 23: 2153.
19. Aharoni, S. M.; Sibilia, J. P. (1979) J. Appl. Polym. Sci. 23: 133.
20. Clarke K, Graves S, Wong A, Triffitt J, Francis M, (1993) J Mater Sci Med. 4: 107.
21. Santos J, Jha L, Monteiro F. (1996) J Mater Sc: Mater Med 7:181.
22. Neo M, Kotani S, Fujita Y, Yamamuro T (1992) J Biomed Mater Res 26:452.